

Residual Stress State after the Laser Surface Remelting Process

Janez Grum and Roman Šturm

(Submitted 14 June 1999; in revised form 11 December 2000)

Residual stresses are a result of elasto-plastic deformations induced in the workpiece material during the heat treatment process. The extent and magnitude of internal stresses depend on temperature conditions in heating and cooling and physical properties of the workpiece material. This contribution discusses the extent and distribution of residual stresses after laser remelting a thin surface layer on ductile iron 80-55-06 (ASTM specification) or Gr 500-7 according to ISO. Residual stresses are not only induced by temperature differences but also result from stresses due to microstructural changes between the surface and the core of the specimen subsequent to cooling to the ambient temperature. The distribution and extent of residual stresses in the remelted thin surface layer depend mostly on melt composition and cooling conditions. Different rates of solidification and subsequent cooling of the remelted layer are reflected in the volume proportions of the created cementite, residual austenite, and martensite in the microstructure. The rate of heating and cooling of the thin surface layer is a function of laser power, beam diameter on the workpiece surface, and interaction time. In addition, the number of passes of the laser beam over the workpiece surface and different degrees of laser trace overlapping were increased to see how these can affect the thermal conditions in the workpiece. To determine the residual stresses, the relaxation method was used. This is based on measuring the specimen strain during electrochemical material removal.

Keywords ductile iron, laser melting, microstructure and residual stress, surface modifications

1. Introduction

Ductile iron is commonly used in a wide range of industrial applications due to its good castability, good mechanical properties, and low price. By varying the chemical and microstructure composition of cast irons, it is possible to change their mechanical properties as well as their suitability for machining. Ductile irons are also distinguished by good wear resistance, which can be raised even higher by additional surface heat treatment. With the use of induction or flame surface hardening, it is possible to ensure a homogeneous microstructure in the thin surface layer; however, this is possible only if cast irons have a pearlite matrix. If they have a ferrite-pearlite or pearlite-ferrite matrix, a homogeneous microstructure in the surface hardened layer can be achieved only by laser surface remelting. Since it has become possible to accurately control the laser beam energy input into the workpiece, a number of authors have successfully applied different thermodynamic models to calculate the temperature cycles in the surface and subsurface layer, from which they defined the depth of the remelted and heat-affected layer.[1–5] The proposed thermodynamic models have enabled optimal selection of heat treatment conditions with respect to the desired depth of the modified layer. In the professional literature, we can find a number of contributions that deal with calculations of residual stresses by the finite element method,[6,7,8] and numerous reports on experimental investigations of residual stresses.[9,10,11] In all of these research studies, measurements of the extent and distribution of residual stresses were made by the x-ray diffraction method. Grum and Šturm[12,13,14] suggested the use of an integrated analysis of the laser-modified layer by the so-called "surface integrity" method, which includes a full description of the modified layer by microhardness measurements and measurements of the size of the remelted and hardened layer, complemented by a complete microstructure analysis supported by x-ray phase analysis and residual stress measurements. The same authors[15,16] also focus attention on the selection of those remelting conditions that will ensure the smallest tensile or higher compressive residual stresses. Only this carefully selected and integrated treatment can contribute to longer lifetime of machine components subjected to dynamical loads.

Janez Grum and **Roman Šturm,** Faculty of Mechanical Engineering, University of Ljubljana, 1000 Ljubljana, Slovenia. Contact e-mail: janez.grum@fs.uni-lj.si.

2. Experimental Procedure

2.1 Material

The flat specimens were made from ductile iron 80-55-06 according to ASTM specification, with a pearlite-ferrite matrix that contained graphite nodules. Its chemical composition in volume percent and the carbon equivalent (CE) are listed in Table 1.

2.2 Remelting Conditions

After laser remelting of a thin surface layer of ductile iron, a thin modified layer consisting of a remelted and hardened layer is obtained. Given that the remelting process was very rapid and the specimen mass sufficiently high, a very rapid cooling was ensured. The actual cooling rates are considerably higher than the required quenching rates and are achieved by

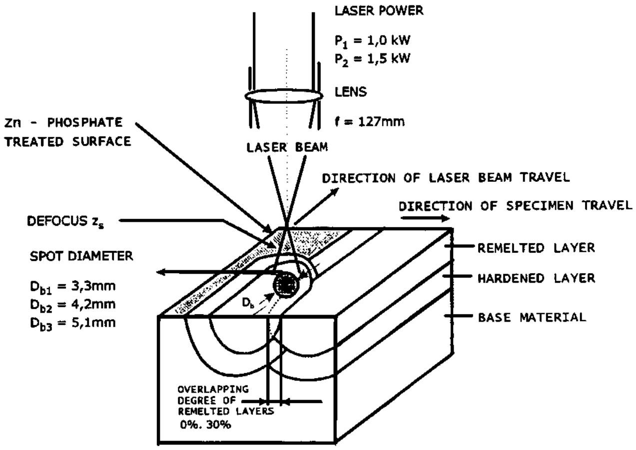

Fig. 1 Laser surface remelting conditions and description of modified specimen surface layer

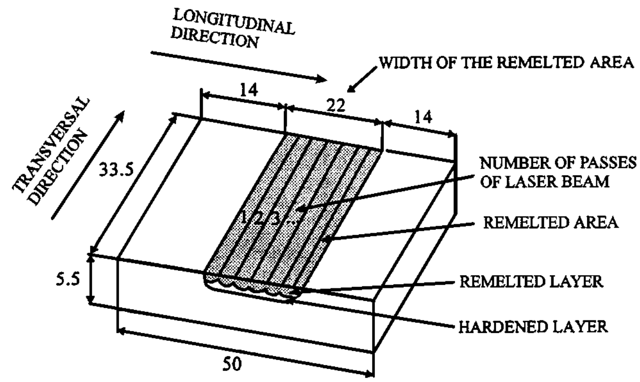

Fig. 2 Laser surface remelting area on the specimen

Table 1 Chemical composition and CE of ductile iron 80-55-06

Chemical composition element (vol.%)					Carbon equivalent
C	Si	Cr	Cu	Mn	CE
3.77	2.26	0.04	0.33	0.13	4.19%

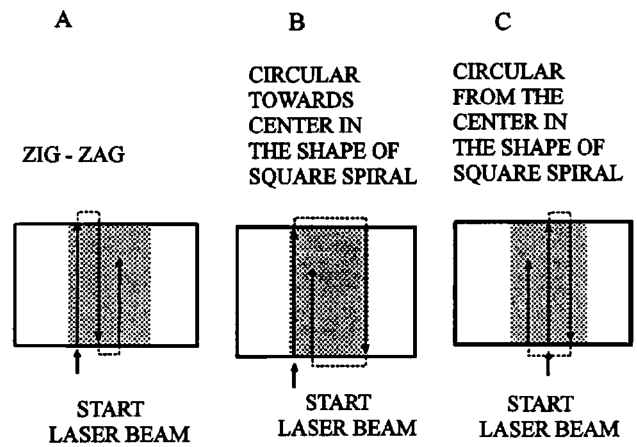

Fig. 3 Different modes of laser beam guiding

thermal conduction into the remaining cold part of the specimen. Due to self-hardening, the process is very clean and simple, which plays an important role in industrial applications. Another important factor in laser machining processes is laser light absorptivity in the interaction with the workpiece surface. This depends on the laser light wavelength, type of workpiece material, and its temperature. Laser light absorptivity of a CO_2 laser of wavelength -10.6 μm is only a few percent and increases to about 50% at the melting temperature. Because of these low values, the specimens were chemically treated in a Zn-phosphate bath at a temperature of 40 °C. In this way, the absorptivity was increased to 80% and a greater depth of the modified layer and repeatability in terms of its size and quality were achieved.

Figure 1 is a schematic presentation of the laser surface remelting process. The selected laser source was a CO_2 laser with a wavelength of $\lambda = 10.6$ μm. Two laser beam power values were chosen, $P = 1.0$ and 1.5 kW. The optical and kinematic conditions were chosen so that the laser remelted the surface layer of the specimen material. The focusing lens has a focal distance $f = 127$ mm and three degrees of defocus $z_{S1} = 22$ mm, $z_{S2} = 28$ mm, and $z_{S3} = 34$ mm. This also defined the size/diameter of the laser beam on the specimen surface, which is $D_{b1} = 3.3$ mm, $D_{b2} = 4.2$ mm, and $D_{b3} = 5.1$ mm. The laser beam scan was $v_{b1} = 15$ mm/s, $v_{b2} = 18$ mm/s, and $v_{b3} = 21$ mm/s. The complete remelting of the specimen surface was ensured by varying the degree of laser trace overlapping, which was adjusted by moving the specimen crosswise to the motion of the laser beam.

Figure 2 gives the dimensions of the specimen and the size of the remelted and hardened surface layer. The laser beam was guided in the transverse direction across the specimen, with the outer laser beam traces being 14 mm away from the specimen edge. The entire width of the modified layer was equal in all experiments irrespective of the energy input. Since the width of the modified layer in a single laser beam passage depends on the degree of defocusing and laser beam scan, in order for each adjacent trace to be modified, it is important that the laser head motion be very accurately defined. Another condition that should be fulfilled is the touching of the remelted traces or their overlapping expressed in percent with respect to the width of a single remelted trace.

Considering the very small depth of the modified surface layer with respect to the specimen thickness, we decided to apply different modes of laser beam guiding across the specimen surface. The chosen modes of laser beam guiding are presented in Fig. 3. Different modes of guiding the laser beam over the specimen surface were selected, *i.e.*, zigzag (A), square-shaped spiral toward the center (B), and square-shaped spiral away from the center (C), with the laser beam turning round outside the specimen to achieve more uniform thermal conditions in the material. In this way, it was possible to achieve different thermal conditions in the thin flat specimen during the remelting

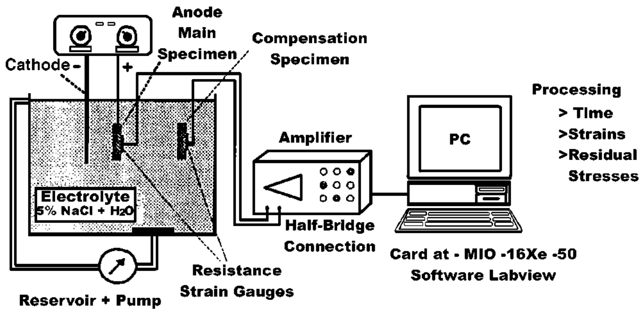

Fig. 4 Experimental system for electrochemical removal of the specimen modified layer and strain measurement with calculation of residual stresses

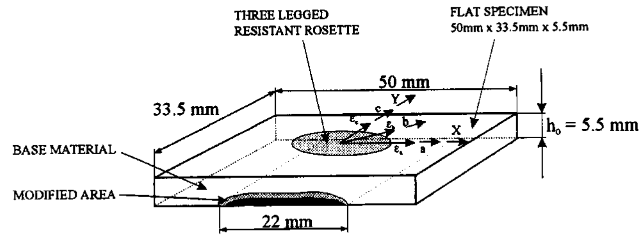

Fig. 5 Modified surface layer area on the specimen and location of the resistance-measuring rosette

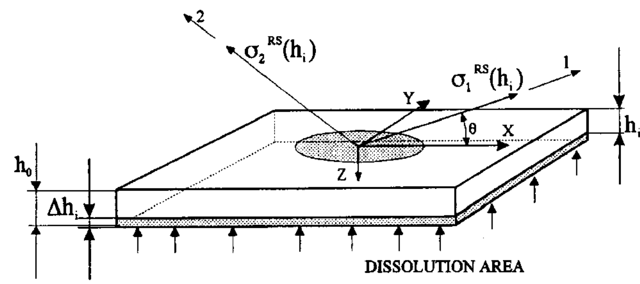

Fig. 6 Dissolution area and location of the resistance measuring rosette with registering particular significant axes

process as well as during cooling, which influence the preheating of the specimen prior to remelting and the tempering of the created modified microstructure. Because of the predefined width of the entire modified surface layer of 22.0 mm, in different laser remelting conditions, different degrees of laser traces overlapping 15 to 22 laser beam passages were made. After each laser beam pass across the specimen surface, the laser beam was turned round 5.0 mm away from the specimen edge. By turning the laser beam round outside the specimen, overheating of the specimen edges was avoided.

To measure the effects of different modes of laser beam scan and the different number of laser beam passes across the surface, thermocouples were placed on the bottom side of the remelted layer so that they registered partial temperature during the heating process.

2.3 Measuring System for Residual Stress Measurements

To measure the residual stresses on thin flat specimens, we decided to use the relaxation method with electrochemical removal of the stressed layer. A result of electrochemical removal of the stressed layer is relaxation and a new mechanical equilibrium state of the specimen. By measuring the strain in a new equilibrium state of the specimen, we can define the stress in the removed layer. Measuring the strain of the specimen after different removal times or different removal depths, we can define the residual stress variation as a function of the modified layer depth. For the calculation of residual stress, it is necessary to know the history of the removal for a given material. In this way, after a certain time of electrochemical removal, it is possible to define the depth of the removal as well as the remaining thickness of the specimen, which is necessary for the calculation of the inertia and resistance moment of the flat specimen. On the basis of the data obtained in this way, we can calculate the extent of residual stresses existing below the surface of the specimen. The experimental system for measuring the strains of the flat specimen after relaxation and the calculation into residual stresses is illustrated in Fig. 4.

The specimen for measuring residual stresses is connected to the anode, whereas the cathode is made of stainless steel. Both electrodes are immersed in an electrolyte containing a 5% water solution of NaCl. Uniform density of the electric current between the anode and the cathode is ensured by a forced circulation of electrolyte and simultaneous filtering of the electrolyte.

On the basis of previous experiments, an optimal time characteristic of the electrochemical removal was defined, which was 0.01 mm/min for the current density 0.5 A/cm^2, and the size of the gap between the electrodes was 3.0 cm.

For continuous measurement of strain of the flat specimen during electrochemical removal of the stressed layer, a three-legged, 45 ° resistance measuring rosette manufactured by Hottinger Baldwin Messtechnik (Darmstadt, Germany), type RY91, was used. The resistance-measuring rosette was placed on the side opposite to the electrochemical dissolution of the specimen. A characteristic of this rosette is that, due to heating of the electrolyte and specimen, another compensation rosette of the same type is necessary in the vicinity of the anode. The compensation resistance-measuring rosette is exposed to the same temperature as the active-measuring rosette, but no force is acting on it or the specimen.

The resistance strain gauge on the specimen and compensation resistance strain gauge were connected in a half-bridging connection so that the difference in the voltage between them was measured considering the compensation of the temperature dilatation of the material. The measured voltage signal was amplified and processed with the AT-MIO-16XE-50 hardware card and LabVIEW software package by National Instruments (Austin, TX) and presented on the screen as the residual stress/depth profile.

Figure 5 and 6 show a specimen made to measure strains connected as anode. The specimen has a length of 50 mm, a width of 33.5 mm, and a thickness of 5.5 mm. The flat specimens were laser remelted in the middle part of the specimen on a length of 22.0 mm and across the entire width of 33.5 mm. On the opposite side of the anode specimen, a 45 ° three-legged

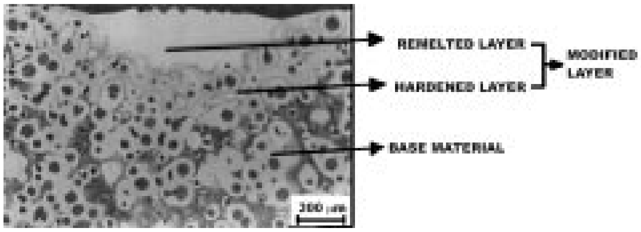

Fig. 7 Cross section of a single laser-modified trace; remelting condition: $P = 1.0$ kW, $z_s = 22$ mm, and $v_b = 21$ mm/s

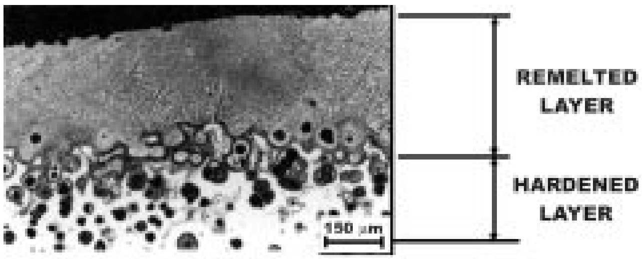

Fig. 8 Laser surface modified layer at 30% overlap of the width of the remelted traces; $P = 1.0$ kW, $z_s = 22$ mm, and $v_b = 21$ mm/s

resistance-measuring rosette was attached in the middle of the specimen with the direction of the strain gauges "a," "b," and "c," as shown in the figure. The electrochemical dissolution was going on across the entire specimen surface. The removal was uniform in time, although the middle part of the specimen with the modified layer and the remaining part to the left and right were in soft state.

Experimental Results

3.1 Microstructure Analysis

After the laser beam had passed across the thin flat specimen, we obtained a microstructurally modified area, the cross section of which was shaped like part of a sphere (Fig. 7). To achieve a uniform thickness of the remelted layer over the entire surface of the flat specimen (Fig. 8), the kinematics of the laser beam were adapted so that a 30% overlapping of width of the remelted traces was ensured.

The microstructure changes in the remelting process of the ductile iron are dependent on temperature conditions during surface layer heating and cooling. In all of the cases of the laser surface remelting process, a modified layer was obtained consisting of two characteristic microstructure layers, *i.e.*, the upper remelted layer and the lower hardened or heat-affected layer.

Remelted Layer

- The microstructure in the remelted surface layer is fine grained and consists of austenite dendrites, with very fine dispersed cementite, together with a small proportion of coarse martensite. X-ray phase analysis of the remelted layer showed the following average volume percentages of the particular phases: 24.0% austenite, 32.0% cementite, 39.0% martensite, and 5.0% graphite (Fig. 9).

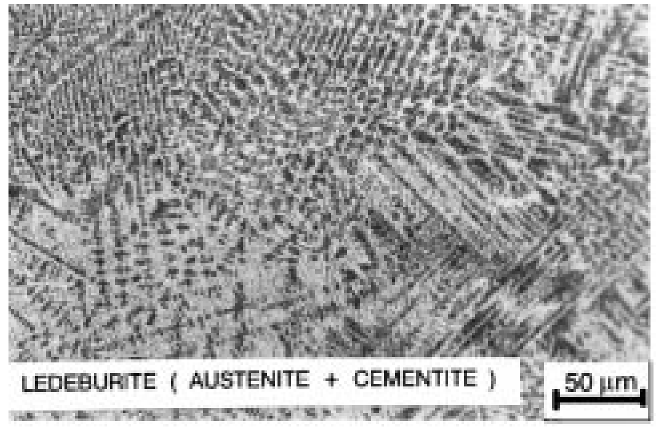

Fig. 9 Microstructure of the remelted layer

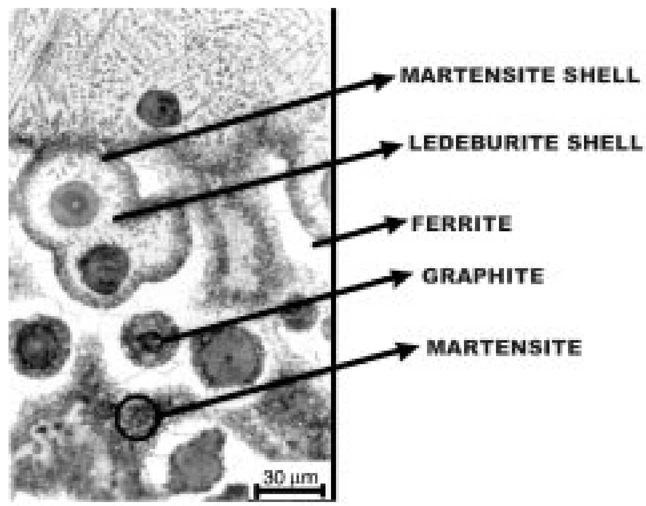

Fig. 10 Microstructure of the hardened layer

- Especially on the surface and to a smaller extent in the immediate subsurface of the remelted layer, a smaller number of graphite nodules are present that represent the remainders of large nodules that have partly dissolved in the melt.

Hardened Layer. In the hardened layer, the heating phase leads to austenitization of the pearlite-ferrite matrix. The austenite matrix also becomes richer in carbon because of the diffusion processes of the latter from graphite nodules. On cooling, the carbon-enriched austenite transforms into martensite and residual austenite, while the austenite with very low carbon content transforms back into ferrite. Figure 10 shows a hardened layer consisting of martensite with a presence of residual austenite, ferrite, and graphite nodules. Graphite nodules are surrounded by ledeburite and/or martensite shells. Typical ledeburite or martensite shells have formed around the graphite nodules. The preconditions for the formation of the ledeburite or martensite shells are a ferrite microstructure around the graphite nodules, heating above the austenitization temperature, and a high-enough cooling rate.

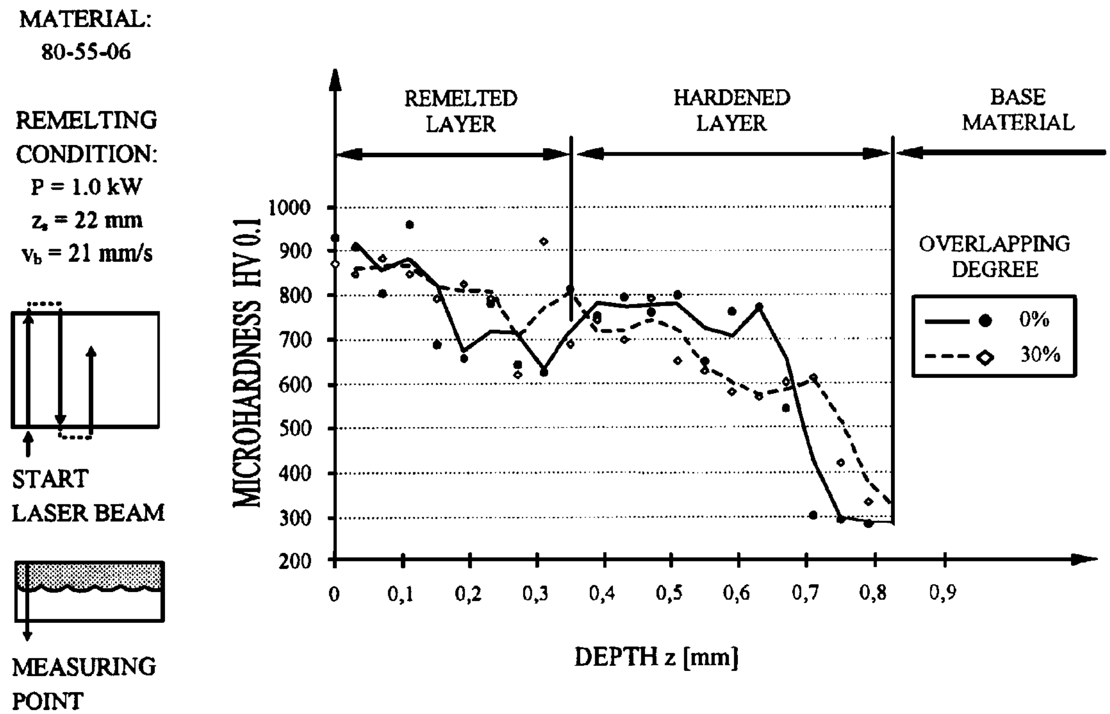

Fig. 11 Microhardness profiles across the laser modified layers at 0 and 30% overlapping degrees

3.2 Microhardness Analysis

Microhardness measurements used a Vickers unit, and the load was 1.0 N. The microhardness of the base material in the soft state ranges between 280 and 300 $HV_{0.1}$ and, after the laser remelting process, increases to 600 to 960 $HV_{0.1}$ across the modified layer. The results of microhardness variation across the modified layer of a given ductile iron are presented in Fig. 10. In the ductile iron, we can note extremely high microhardness around 960 $HV_{0.1}$ on the surface of the remelted layer, which falls uniformly to the value 570 to 610 $HV_{0.1}$ in the hardened layer. The drop in microhardness then reoccurs at a depth of the remelted layer $d_R = 0.28$ mm at zigzag laser beam scan mode, which is attributed to changes in austenite to martensite.

Figure 11 also presents a comparison of microhardness profiles subsequent to surface remelting by a single trace and by several overlapping traces. The results of microstructure analysis and the measured microhardness across the modified layer confirm that, in surface remelting, by overlapping the remelting traces, we achieve the effect of annealing of martensite microstructure in ductile iron and, due to that, the lowering of the microhardness.

3.3 Influence of Time-Temperature Variation on the Size of the Remelted and Hardened Layers

Figure 12 shows different modes of laser beam scan across the flat specimen surface and the time-temperature variation in the bottom side of the specimen. The time-temperature variation gives information on the temperature changes in heating and cooling of the material on the bottom side of the specimen. Considering the three different modes of laser beam scan across the specimen surface, we can state the following.

- The lowest maximum temperature on the bottom side of the specimen is reached with the circular mode of laser beam scan in the shape of the square spiral, starting in the middle and ending on the edges of the remelted area.
- Somewhat higher temperatures of the material are achieved by zigzag laser beam scan.
- The highest maximum temperature in the material on the bottom side of the remelted layer is achieved with the circular mode of laser beam scan in the shape of the square spiral, starting on the edges of the remelted layer and ending in the middle of the remelted area.

Each laser beam passage across the specimen surface induces gradual heating of the material on the bottom side of the remelted layer, the result of which is preheating of the material before the next passage. The increased temperature of the specimen makes the yield point of the material slightly lower, which may, with the given internal stresses, result in greater deformation of the specimen and a lower residual stress.

Table 2 presents some typical dimensions of the modified layer as a function of selected remelting conditions. As we can see, the amount of the energy supplied changes from 14.4 to 16.3 J/mm^2, affecting the increase of the depth of the modified layer.

In Fig. 12, the measurements of the depths of the modified layer are presented for different modes of laser beam scan and different surface remelting conditions. The influence of preheating the specimen with different modes of laser beam scan across the specimen surface shows in the depth of the

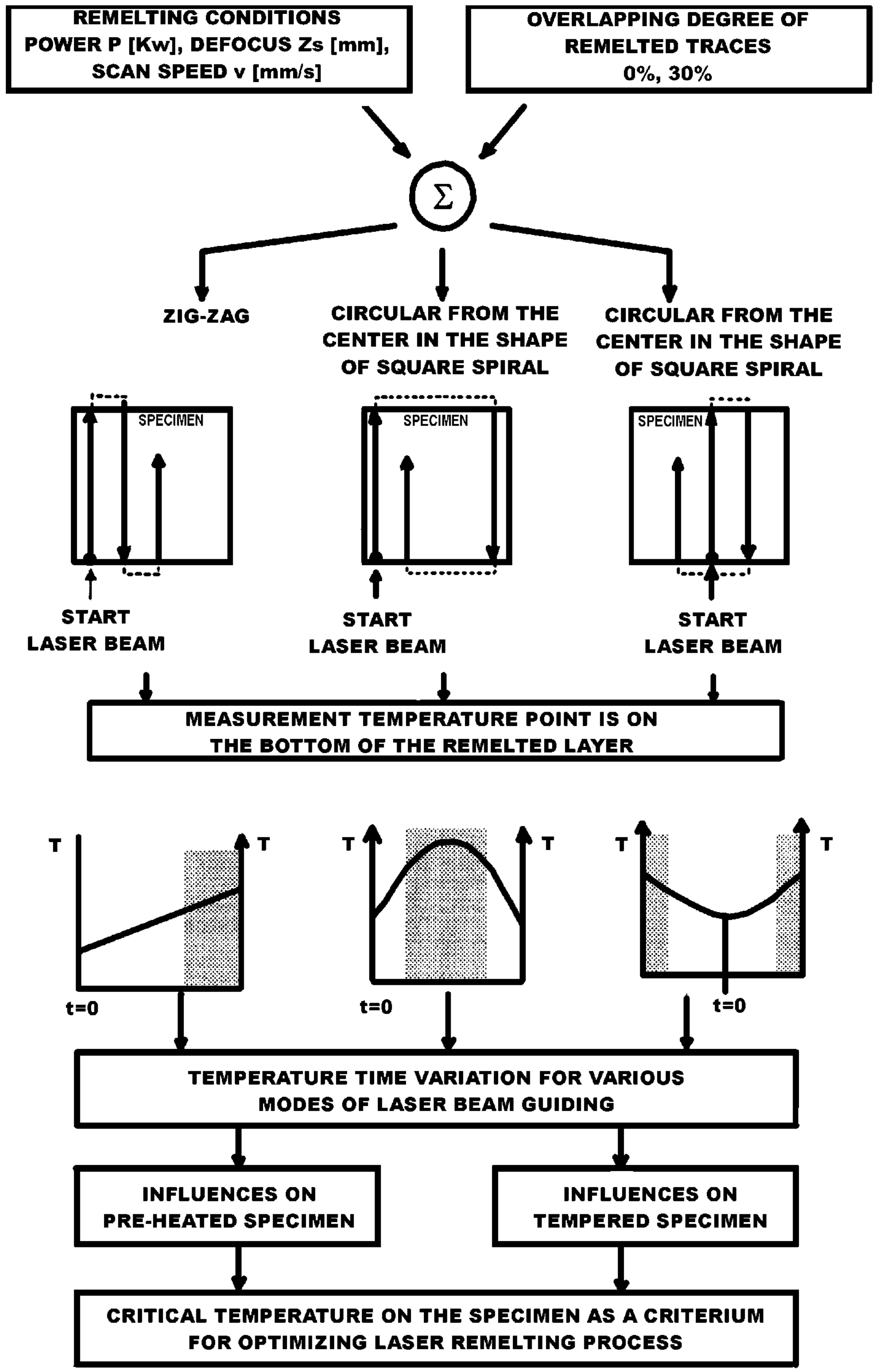

Fig. 12 Selected modes of laser beam guiding across the flat specimen surface

remelted layer d_R and in the depth of the modified layer d_M, respectively. In the comparison of the influences of preheating, two remelting conditions, *i.e.*, the lowest energy input $E_i = 14.4$ J/mm^2 and the highest one $E_i = 16.3$ J/mm^2, were also included.

The table below Fig. 13 gives data on the depth of the remelting layer d_R and on the depth of the modified layer d_M for three selected measuring points. Figure 14 shows a macrophoto of the specimen in cross section. The specimen was laser remelted at the following conditions: $P = 1$ kW, $D_b = 3.3$ mm, and $v_b = 21$ mm/min at circular laser beam guiding from the center in the shape of square spiral across the specimen surface. The depth of the remelted layer is 0.28 mm

Table 2 Dimensions of a single laser modified trace at given remelting conditions

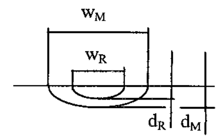

Processing parameters: Power P, defocus z_s, scan speed v_b	Spot diameter D_b (mm)	Energy input E_i (J/mm^2)	Dimensions: Remelted layer, Depth d_R (mm)	Remelted layer, Width w_R (mm)	Modified layer, Depth d_M (mm)	Modified layer, Width w_M (mm)
P = 1.0 kW, z_s = 22 mm, v_b = 21 mm/s	3.3	14.4	0.27	1.01	0.54	1.84
P = 1.0 kW, z_s = 28 mm, v_b = 15 mm/s	4.2	15.8	0.31	1.67	0.68	2.4
P = 1.0 kW, z_s = 34 mm, v_b = 18 mm/s	5.1	16.3	0.41	2.03	0.82	3.18

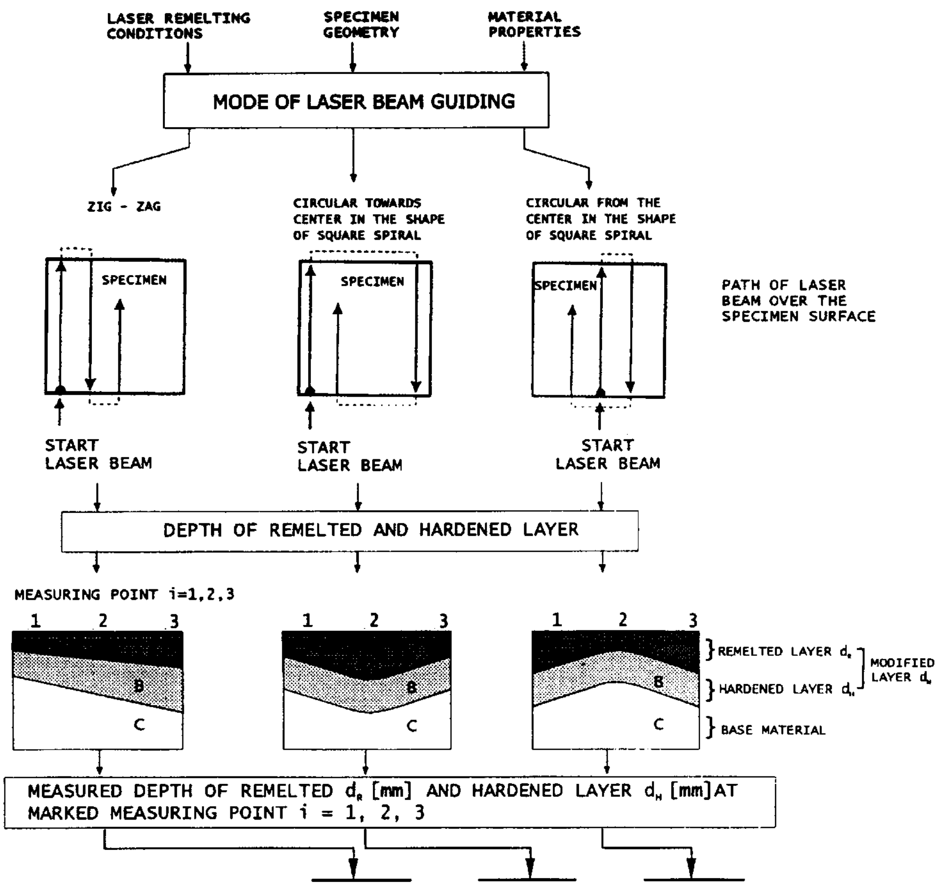

MEASURING POINT	i	1	2	3	1	2	3	1	2	3	REMELTING CONDITION
DEPTH OF THE REMELTED LAYER	d_R [mm]	0.28	0.31	0.35	0.33	0.41	0.28	0.4	0.31	0.38	P = 1.0 kW, D_b = 3.3 mm,
DEPTH OF THE MODIFIED LAYER	d_M [mm]	0.6	0.67	0.75	0.65	0.85	0.57	0.75	0.64	0.68	V_b = 21 mm/s, E_i = 14.4 J/mm^2
DEPTH OF THE REMELTED LAYER	d_R [mm]	0.45	0.5	0.55	0.45	0.55	0.37	0.43	0.4	0.44	P = 1.5 kW, D_b = 5.1 mm,
DEPTH OF THE MODIFIED LAYER	d_M [mm]	0.85	0.91	0.97	0.85	1.2	0.73	0.85	0.8	0.85	V_b = 18 mm/s, E_i = 16.3 J/mm^2

Fig. 13 Depth variation of the remelted and modified layer on ductile iron 80-55-06 achieved under the given remelting conditions

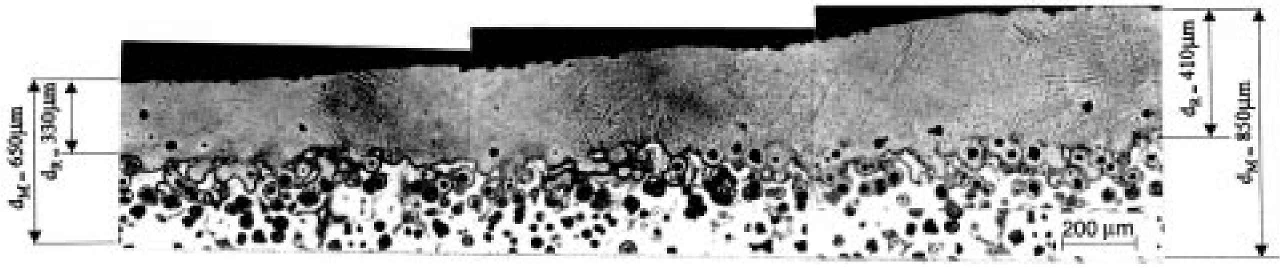

Fig. 14 Macrophoto cross section with variation depths of the remelted layer

at measuring point "1" and 0.35 mm at measuring point "2." The data given are taken from Fig. 13.

3.4 Calculation of Residual Stresses

The method for measurement of residual stresses consists of removing a thin stressed surface layer of Δh_i thickness on the one face of the specimen that was laser remelted.[17] A new equilibrium state is thus established involving the specimen strain and a new stress distribution. The principle of the present method is to connect measured strains to calculate the residual stresses at relaxation of the specimen by electrochemical dissolution.

Strains (ε_a, ε_b, and ε_c) of the resistance measuring rosette in the direction of individual legs were measured. One leg of the resistance measuring rosette "a" was positioned perpendicular to the direction of the surface remelting layer (perpendicular to the path of the laser scan), the second one "b" at an angle of 45° to the direction of remelting, and the third one "c" in the direction of remelting (Fig. 5 and 6). The specimen plane in which the three-legged resistance rosette was placed was defined by the rectangular *X–Y* coordinate system. The resistance measuring rosette was positioned at the specimen so that the coordinate axes *X* and *a*, and *Y* and *c*, agreed. After electrochemical dissolution of the thin surface layer Δh_i at the modified surface layer, a new equilibrium state was established, which included strain and a new stress distribution. The method of calculating residual stresses was based on the data of the strains measured with the known new specimen thickness h_i and after taking away the layer thickness Δh_i.

The method of calculating residual stresses is based on the following assumptions:

- The thickness of the dissolved layer Δh_i should be very small in comparison to the other specimen dimensions so that the expression $(\Delta h_i)^{-2}$ can be neglected. This is a necessary condition in order to presume the plane stress condition σ_α^{RS} where $\sigma_x \neq 0$, $\sigma_y \neq 0$, and $\sigma_z = 0$. σ_α^{RS} = the principal residual stresses (MPa), and α = the principal directions 1 and 2.
- In each dissolved layer, Δh_i residual stresses are independent of directions *X* and *Y* and change only in linear dependence on the depth $\Delta\sigma_\alpha^{RS} = f(z)$, which indicates that the residual stresses occurring in the *X-Y* plane are isotropic.
- For the strains produced by electrochemical dissolution, a linear dependence of residual stresses released in accordance with Hook's law is presumed.
- Strains in the direction of the leg axes were measured (ε_a, ε_b, and ε_c) with the three-legged resistance measuring rosette. The extent of the principal strains ε_a, *i.e.*, ε_1 and ε_2, could be determined from the measured strains:[17,18]

$$\varepsilon_1 = \frac{1}{2} \cdot \left(\varepsilon_a + \varepsilon_c + \sqrt{(\varepsilon_a - \varepsilon_c)^2 + (2 \cdot \varepsilon_b - \varepsilon_a - \varepsilon_c)^2}\right) \quad \text{(Eq 1)}$$

$$\varepsilon_2 = \frac{1}{2} \cdot \left(\varepsilon_a + \varepsilon_c - \sqrt{(\varepsilon_a - \varepsilon_c)^2 + (2 \cdot \varepsilon_b - \varepsilon_a - \varepsilon_c)^2}\right) \quad \text{(Eq 2)}$$

With regard to the fixed rectangular *X-Y* coordinate system of the specimen, the position of the principal residual stresses was also defined. Thus, angle θ between the fixed axis *X* and the movable axis 1 was determined:

$$\theta = \frac{1}{2} \cdot \arctan\left(\frac{2 \cdot \varepsilon_b - \varepsilon_a - \varepsilon_c}{\varepsilon_a - \varepsilon_c}\right) \quad \text{(Eq 3)}$$

The result of the calculation is expected to represent the principal residual stresses distribution:

$$\sigma_\alpha^{RS}(h_{j-1}) = \frac{-(h_{j-1} - \Delta h_j)^2}{2 \cdot (h_{j-1} + 2 \cdot \Delta h_j) \cdot h_j} \cdot B_{j,\alpha} - \sum_{j-1}^{j-1}\left[-3 \cdot \frac{(h_{j-1} + \Delta h_i)}{(h_{i-1} - \Delta h_i) \cdot (h_{i-1} + 2 \cdot \Delta h_i)} \cdot h_{j-1} + 1\right] \cdot B_{i,\alpha} \quad (\alpha = 1, 2) \quad \text{(Eq 4)}$$

where *E* is the Young's modulus; *v* is Poisson's ratio; h_i is the thickness of the specimen; Δh_i is the thickness of the dissolved layer; and $\Delta\varepsilon_a$, $\Delta\varepsilon_b$, and $\Delta\varepsilon_c$ are the differences of the strains resulting from thin surface layer dissolution.

The stress $B_{j,\alpha}$, *i.e.*, ($B_{j,1}$, $B_{j,2}$), can be calculated after each dissolution of material thickness Δh_j on the basis of the difference of the strains of the specimen $\Delta\varepsilon_{j,1}$ and $\Delta\varepsilon_{j,2}$:

$$B_{j,1} = \frac{E}{1 - v^2} \cdot (\Delta\varepsilon_{j,1} + v\Delta\varepsilon_{j,2}) \quad \text{(Eq 5)}$$

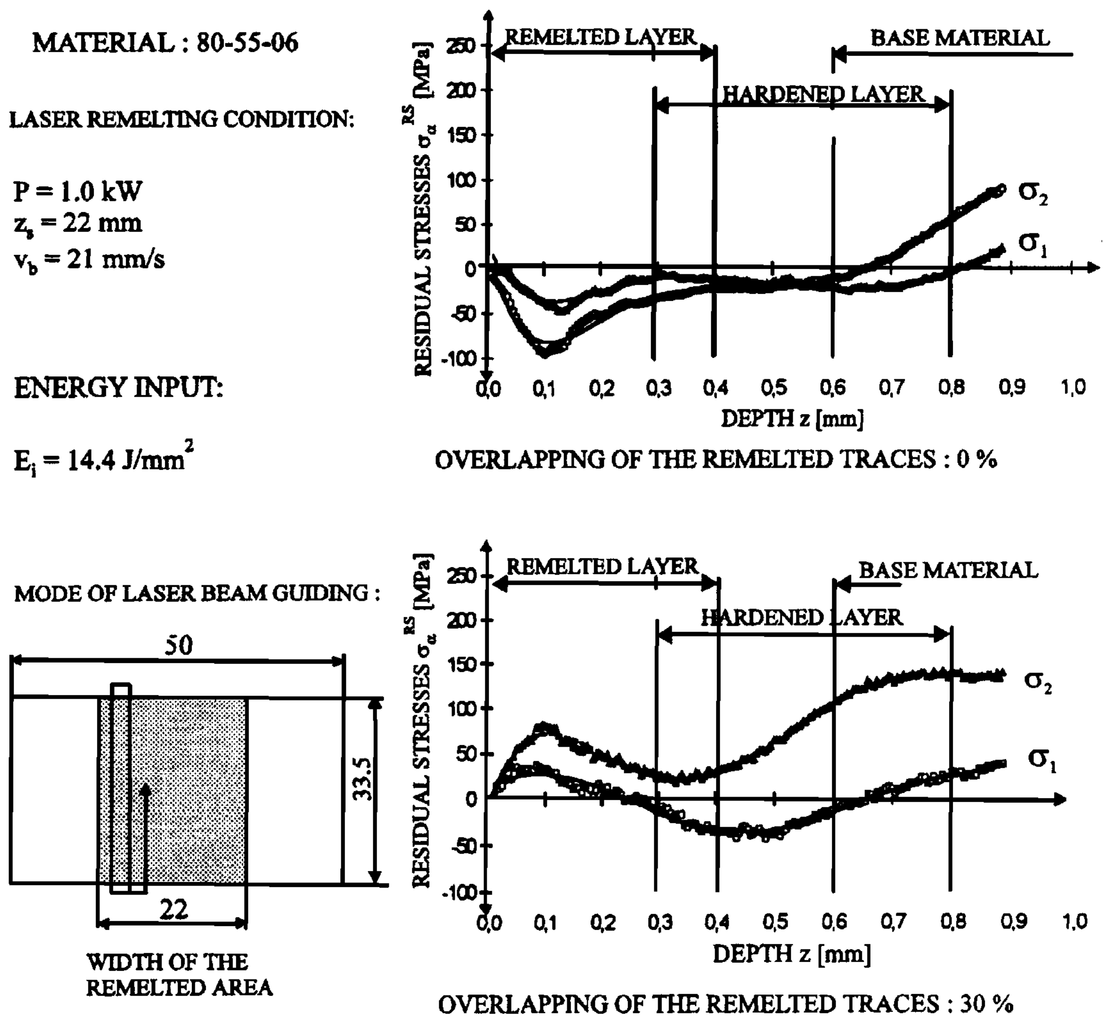

Fig. 15 Residual stresses in ductile iron 80-55-06; zigzag laser beam guiding at given laser remelting conditions

$$B_{j,2} = \frac{E}{1 - \nu^2} \cdot (\Delta\varepsilon_{j,2} + \nu\Delta\varepsilon_{j,1}) \qquad \text{(Eq 6)}$$

Taking into account the specimen thickness prior to the electrochemical dissolution and the thickness of the dissolved layer permitted calculation of residual stresses at a certain specimen depth (first term of Eq 4). This, however, was not the real state of residual stresses in the depth (h_j). In the calculation of the real state of residual stresses in the depth (h_j), the stress states ($B_{j,1}$) and ($B_{j,2}$) in the initially removed material layers, *i.e.*, all ($j - 1$) layers (second term of Eq 4), should also be taken into account.[17,18]

3.5 Residual Stresses Analysis

With the resistance measuring strain gauges on the rosette, the strains were measured in the directions *a*, *b*, and *c*, and then, using the software support, the principal residual stresses σ_1 and σ_2 and angle θ between the principal stress σ_1 and the longitudinal *X*-axis of the specimen were calculated.

Figure 15 shows the results of calculations of principal residual stresses in the thin surface layer with the zigzag laser beam guiding at the 0 and 30% overlapping of the remelted layer. We can state the following.

- Residual stresses σ_1 are directed in the longitudinal direction of the specimen and are, in this case, smaller than residual stresses σ_2 directed in the transverse direction of the specimen.
- During the process of laser surface remelting, the specimen bends more in the longitudinal direction than in the transverse direction. This causes additional lowering of tensile residual stresses in the modified layer.
- At 0% overlapping of the remelted layer, the compressive residual stresses were achieved in the thin surface layer in the longitudinal and transverse directions ranging between 100.0 and −5.0 MPa. These change into tensile residual stresses in the transition area from the hardened layer into the matrix. A higher 30% overlapping induces the occurrence of tensile residual stresses with maximum values to

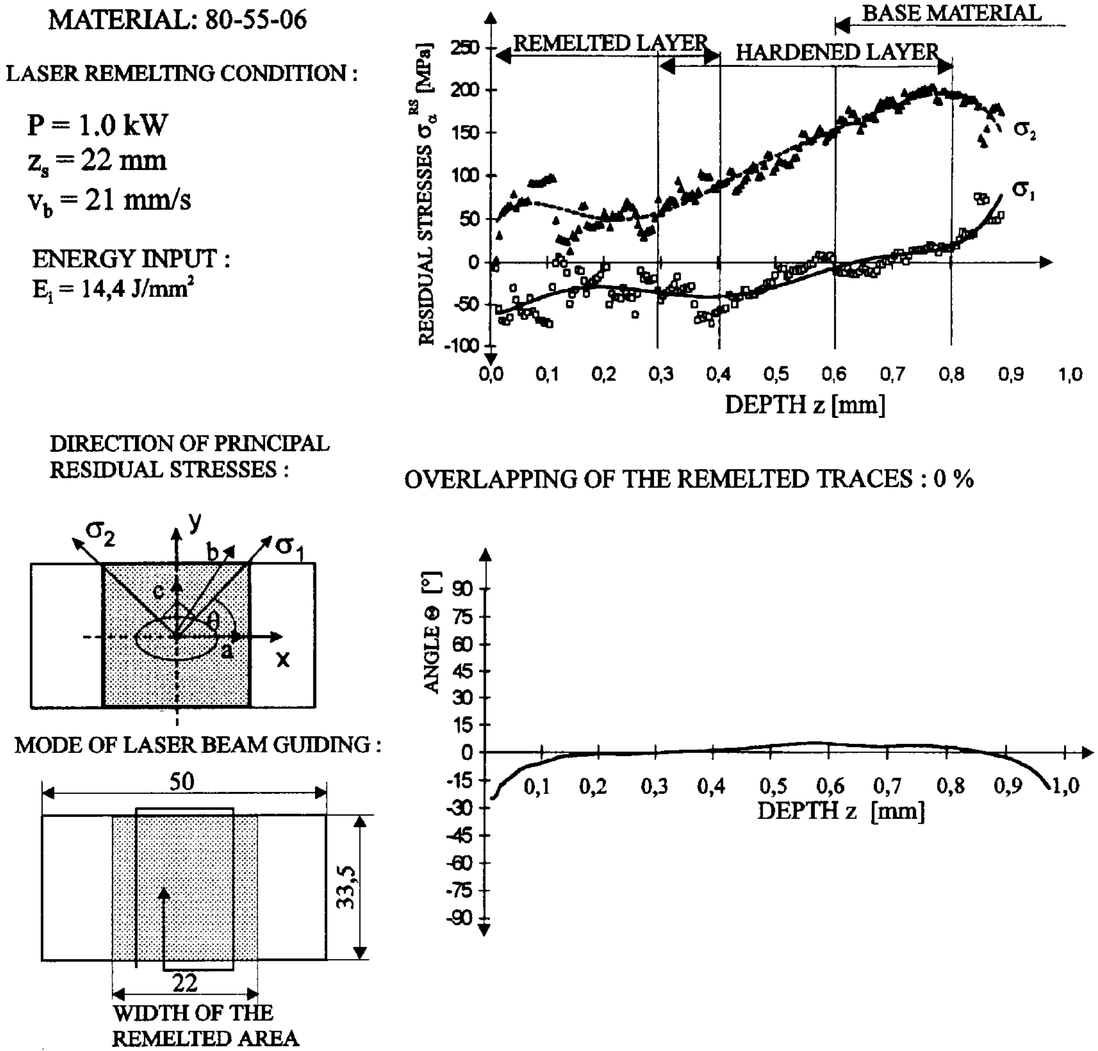

Fig. 16 Residual stresses in ductile iron 80-55-06 with a circular laser beam guiding in the shape of a square spiral beginning on the edge of the remelted area and ending in the middle of the specimen at the above indicated laser remelting condition

+90 MPa in the remelted layer, which then change into compressive residual stresses with a maximum value of 50 MPa in the hardened layer.

Figure 16 shows the results of measurements of principal residual stresses in the thin surface layer with a laser beam guiding in the shape of a square spiral beginning on the edge of the remelted area and ending in the middle of the specimen at given laser remelting conditions.

We can see the size and distribution of the calculated principal residual stresses as a function of depth and the direction angles of the principal residual stresses with respect to the longitudinal *X*-axis of the specimen. In the given case, the hardening procedure was carried out so that the hardening traces touched each other on the surface, which means a 0.0% overlapping of the remelted traces. The residual stresses were measured to the depth of 0.9 mm, which means that they were measured to the transition of the modified layer into the matrix.

From the results of the measured strains of the flat specimen during laser surface remelting as well as from the results of calculated residual stresses in the thin surface layer, the following conclusions can be drawn.

- The principal residual stresses σ_1 are directed perpendicularly to the direction of the laser path, whereas the principal residual stresses σ_2 are directed in the direction of the laser path.
- The principal residual stresses σ_2 acting in the direction of laser remelting and being of tensile nature are much higher than the residual stresses σ_1 acting perpendicularly to the direction of laser remelting and are prevailingly compressive over the entire modified layer.
- The principal residual stresses σ_1 are reduced already during the process of laser surface remelting due to lowering the yield strength of the material, which, due to the temperature field, causes bending of the specimen, as seen

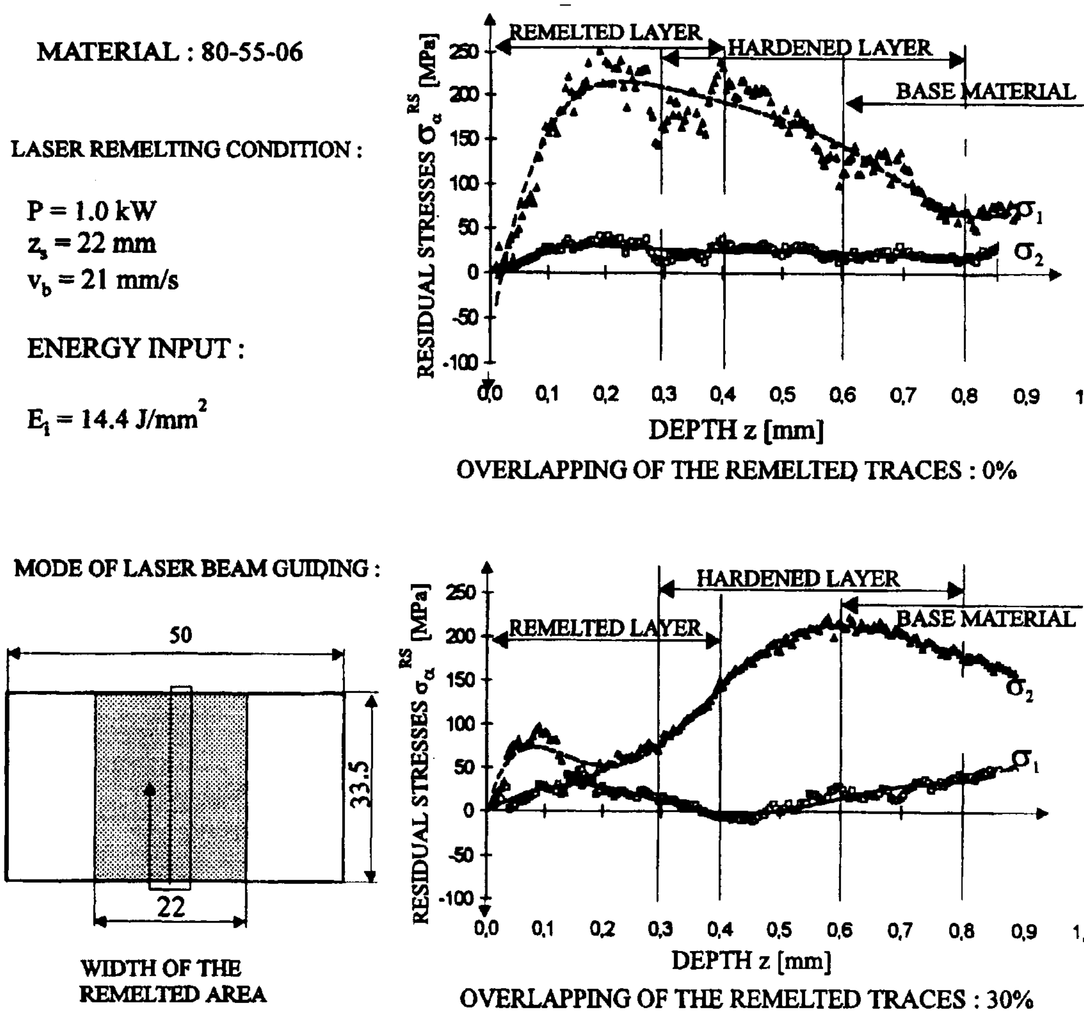

Fig. 17 Residual stresses in ductile iron 80-55-06 with a circular laser beam guiding in the shape of a square spiral starting in the middle of the specimen and ending on the edge of the remelted area at the above indicated laser remelting condition

from the top. The specimen undergoes convex bending in the longitudinal direction, which causes a reduction in tensile residual stresses in the modified surface layer. In the transverse direction, the specimen suffers a considerably smaller deformation or even a slight concave bending, which causes an increase in tensile residual stresses σ_2.

- The sizes of the measured strains or residual stresses calculated from them are also influenced by the unmelted layer on the outer sides of the specimen. Due to convex bending of the specimen during the laser remelting process, the unmelted layer of the material contracted, thus inducing small residual stresses of compressive nature.
- Residual stresses in the modified surface layer in the longitudinal direction of the specimen are compressive and range between 80.0 and 5.0 MPa when, in the transition area from the hardened layer to the matrix, they change into tensile residual stresses. In the transverse direction of the specimen, residual stresses are always tensile and range from +50 to +200.0 MPa in the modified layer.

Figure 17 shows the results of calculated principal residual stresses in the thin modified surface layer for the case of circular laser beam scan in the shape of a square spiraling beginning in the middle of the flat specimen and ending on the edge of the remelted layer for 0 and 30% overlapping degrees of the individual remelted traces.

From the calculated values and distribution of the principal residual stresses at a circular laser beam scan ending in the middle of the specimen, we can see that, in comparison with the other modes of guiding the laser beam across the surface, it is possible to achieve slightly higher tensile residual stresses in the thin surface layer. This increase in tensile residual stresses is largely a function of the maintained high rate of cooling across the entire remelted layer in the course of the laser remelting process, which can be explained by the fact that the input heat energy is immediately transferred into the cold surrounding material.

Considering the calculated values and distribution of residual stresses at zigzag mode of laser beam scan, we can state the following.

- The increased bending of the specimen caused by surface layer remelting results in reduction of tensile residual stresses in the modified surface layer.
- An increased degree of overlapping of the remelted trace results in lowering residual stress values in the thin surface remelted layer.

Based on the measured specimen strains and calculated principal residual stresses σ_1 and σ_2, we can note that, in laser remelting of a thin surface layer on thin flat specimens of small size, there is a strong tendency of specimen bending in the direction transverse to the laser path, *i.e.*, in our case, along the length of the specimen.

4. Conclusions

The process of laser surface remelting induces residual stresses in the modified surface layer. Phase transformations causing the volume decrease of the remelted layer give rise to tensile residual stresses in it. On the other hand, in the hardened layer, martensite transformation causes an increase in volume and gives rise to compressive residual stresses. From experiments, it has been concluded that the distribution of residual stresses is largely dependent on the cooling rate of the laser-modified layer whose change may cause the formation of different microstructures, at various overlapping degrees of remelted traces. With different overlapping degrees of remelted traces, it is possible to achieve a release of microstructure residual stresses in the transition zone and, at the same time, preheating of the material for the next trace, which affects the rate of cooling within the modified layer. Experiments have proved that the cooling rate of thin specimens can be influenced by the choice of the laser beam scan, different degrees of remelted traces, and a different choice of remelting conditions. Remelting conditions can be chosen by changing the laser beam power, defocusing the degree reflected in the laser beam diameter on the specimen surface, and adjusting the scan speed of the beam. All of these laser-remelting conditions, each in its own way, change the amount of the energy input and can have an important effect on the size and quality of the modified layer and residual stresses. A greater amount of input energy into the specimen results in a higher increase of temperature in it and higher overheating of the specimen, which, on the other hand, lowers the cooling rate in the modified layer and gives rise to the occurrence of small microstructure residual stresses in this layer.

References

1. D. Rosenthal: *Trans. ASME,* 1946, Nov., pp. 849-66.
2. H.S. Carslaw and J.C. Jaeger: *Conduction of Heat in Solids,* 2nd ed., 1959, Clarendon Press, Oxford, United Kingdom, 1986.
3. H.E. Cline and T.R. Anthony: *J. Appl. Phys.,* 1977, vol. 48 (9), pp. 3895-3900.
4. M. Bass: in *Laser Heating of Solids,* M. Bertolotti, ed., Plenum Press, New York, NY, 1983, pp. 77-115.
5. E. Geissler and H.W. Bergmann: “Calculation of Temperature Profiles, Heating and Quenching Rates during Laser Processing,” B.L. Mordike, ed., Papers presented at the *Eur. Conf. on Laser Treatment of Materials 1986,* Bad Neuheim, Germany, Deutsche Gesellschaft für Metallkunde E.V., DGM Informationgeselschaft mbH, Oberursel, Germany, 1987, pp. 101-14.
6. M. de Freitas, M.S. Pereira, H. Michaud, and D. Pantelis: *Mater. Sci. Eng.,* 1993, vol. A167 (1–2), pp. 115-22.
7. S. Denis, A. Simon, and G. Beck: in *Analysis of the Thermomechanical Behaviour of Steel during Martensitic Quenching and Calculation of Internal Stresses,* E. Macherauch and V. Hauk, eds., Eigenspannungen: Entstehung-Messung-Bewertung, Deutche Gesellschaft für Metallkunde E.V., Oberursel, Germany, 1983, Band 1, pp. 211-37.
8. D. Grevey, L. Maiffredy, and A.B. Vannes: *J. Mech. Working Technol.,* 1988, vol. 16 (1), pp. 65-78.
9. Y.S. Yang and S.J. Na: *Surf. Coating Technol.,* 1989, vol. 38 (3), pp. 311-24.
10. Y.S. Yang and S.J. Na: *Surf. Coatings Technol.,* 1990, vol. 42 (2), pp. 165-74.
11. J. Domes, D. Müller, and H.W. Bergmann: *ECLAT ’88,* Deutscher Verlag fur Schweisstechnik (DVS) GmbH, Dusseldorf, Germany, 1988, 163, pp. 272-77.
12. J. Grum and R. Šturm: *J. Mech. Eng., Ljubljana,* 1995, vol. 41 (11–12), pp. 371-80.
13. J. Grum and R. Šturm: *Proc. Conf. “MAT-TEC 96,”* Subject Editor: Jian Lu, Technology Transfer Series, Series Editor; A. Niku-Lari, IITT International, Gournay Sur Marne, Paris, France, 1996, pp. 185-93.
14. J. Grum and R. Šturm: *Proc. Conf. “Quenching’ 96,”* Cleveland, OH, ASM International, Materials Park, OH, 1996, pp. 193-200.
15. J. Grum and R. Šturm: *Surf. Coatings Technol.,* 1997, vol. 100–101, pp. 455-58.
16. J. Grum and R. Šturm: *J. Mater. Eng. Performance,* 2000, vol. 9 (2), pp. 138-46.
17. S. Hariri, R. Vaucher, P. Flahaut, D. Eyzop, and C. Robin: *Proc. Int. Conf.* “MAT-TEC’ 96,” Subject Editor: Jian Lu, Technology Transfer Series, Series Editor; A. Niku-Lari, IITT International, Gournay Sur Marne, Paris, France, 1996, pp. 111-18.
18. R. Šturm: Ph.D. Thesis, University of Ljubljana, Ljubljana, 1998.